Optik 127 (2016) 11161–11172

Contents lists available at ScienceDirect

Optik

journal homepage: www.elsevier.de/ijleo

Original research article

Numerical simulation and designing artificial neural network for estimating melt pool geometry and temperature distribution in laser welding of Ti6Al4V alloy

Mohammad Akbari[a,*], Seyfolah Saedodin[b], Afshin Panjehpour[a], Mohsen Hassani[a], Masoud Afrand[a], Mohammad Javad Torkamany[c]

[a] Department of Mechanical Engineering, Najafabad Branch, Islamic Azad University, Najafabad, Iran
[b] Faculty of Mechanical Engineering, Semnan University, Semnan, Iran
[c] Iranian National Centre for Laser Science and Technology (INLC), P.O. Box 14665-576, Tehran, Iran

ARTICLE INFO

Article history:
Received 3 June 2016
Accepted 12 September 2016

Keywords:
Weld geometry
Temperature distribution
Numerical simulation
Artificial neural network

ABSTRACT

Weld geometry is a critical factor for determining the quality of Ti6Al4V welded joints. The size of the weld cross section profile has been quantitatively investigated through experimental and numerical analysis. Due to the difficulties in temperature measuring of the molten pool region, the temperature distribution through numerical simulation was exerted as an indirect approach for estimating the size of the melt pool profile and HAZ region. Moreover, the numerical model was used for prediction of cooling rate in the melt pool and thereby characterization of fusion zone microstructure. To achieve an accurate prediction of the weld geometry at low time and cost, the process was simulated based on artificial neural network. Different ANNs were developed for progressive prediction of the weld pool temperature distribution and weld geometry. Two feed-forward back propagation neural network models with 11 and 14 neurons were developed to predict optimum process parameters. The proposed artificial neural network models perfectly predicted the process with mean square errors of 0.079 and 0.063. The results indicated that ANN outputs were in good agreement with the experimental and numerical data.

1. Introduction

Laser welding has great benefits such as rapid processing capability, high speed, deep penetration and good precision. Laser welding of titanium alloys is preferred due to the high efficiency and low production costs of welding techniques which have been widely used in aerospace, biomedical and power generation industries. Titanium alloys have excellent mechanical properties and good corrosion resistance at the elevated temperatures but have some difficulties by conventional welding methods. Weld geometry is a predominant factor in efficiency of laser welding process. Various studies were conducted to predict the weld geometry through different methods such as numerical simulations, artificial intelligence, design of experiments and etc. [1–4]. Gao et al. considered the influence of weld cross-section profiles and microstructure on properties of pulsed Nd:YAG laser welding of Ti6Al4V sheet under different welding conditions. They remarked that different joint shapes were under different heat input and thereby different resultant tensile strength [5]. Xu et al. [6] investigated the

* Corresponding author at: Department of Mechanical Engineering, Najafabad Branch, Islamic Azad University, Najafabad, Iran.
E-mail address: m.akbari.g80@gmail.com (M. Akbari).

http://dx.doi.org/10.1016/j.ijleo.2016.09.042
0030-4026/

Nomenclature

ANN	Artificial neural network
V	Welding speed (mm/s)
TC	Temperature center (°C)
TA	Temperature around (°C)
HAZ	Heat affected zone
FZ	Fusion zone
BM	Base metal
FFBP	Feed forward back propagation
H_1	Total width (mm)
H_2	Depth of fusion zone (mm)
H_3	Width of fusion zone (mm)
MSE	Mean square error (%)
MAPE	Mean absolute percentage error
APE	Absolute percentage error

microstructure characterization of the Ti6Al4V laser welded zones. A 2-D thermal-structural finite element model was used to simulate the quasi-steady-state laser welding process. They found that microstructure transformation was affected by the cooling rate through the variation of laser welding speed. Mi et al. [7] developed a coupled thermal and metallurgical model for simulation of temperature distribution and phase transformation during the tungsten inert gas (TIG) welding of Ti6Al4V alloy. The thermal properties were characterized based on the phase fractions and the thermal properties of each pure phase. The Comparison of the results of these models with the measurements showed that the model considered the effect of solid phase transformations which described the temperature profile during cooling accurately. Dissimilar butt welding of Ti6Al4V to the pure niobium was performed using a pulsed Nd:YAG laser by Torkamany et al. [8]. They investigated the effects of laser process parameters on the melt profile on both sides of the weld line by considering the thermo-physical properties of the base metals. A sound weld with full penetration along the dissimilar interface was obtained through optimization of the process parameters. A three-dimensional transient numerical model was carried out by Wang et al. They studied the temperature field and molten pool shape during continuous laser keyhole welding of 304 stainless steel sheet [9]. The enthalpy-porosity technique was used to account the latent heat during melting and solidification. Temperature fields and weld pool shape were calculated using FLUENT software. The calculated weld dimensions showed acceptable agreement with the experimental results. Wei et al. studied mechanical properties of HAZ region during laser welding of DP600 steels within thermal simulated method. The simulation thermal histories in different regions of HAZ were correlated with thermocouples measurements. They showed that the thermal histories in weld and HAZ were very sensitive to the distance from the weld centerline, which resulted in different microstructures and mechanical properties. Therefore, it represented the decreasing trend of the tensile strength with increasing the distance from the weld centerline [10]. Artificial neural network (ANN) is one of the most applicable models for nonlinear analysis due to the significant advantages of high accuracy, low cost and time. An ANN is a parallel processing network which used for determining the complex nonlinear relationships between parameters and prediction of output variables [11,12]. In recent years, some researchers have applied ANNs for modeling and prediction of process parameters in different applications [13–17]. Sathiya et al. [18] developed a model based on the artificial neural network to predict weld geometry (width and depth) and tensile strength of the laser welded butt joints of AISI 904L. ANN was used for establishment of the relationship between the laser welding input parameters and the weld geometry in three different shielding gases (argon, helium and nitrogen). The proposed model was used for optimization of the process parameters base on the genetic algorithm. Their results showed that the theoretically model was in good agreement with the experimentally obtained results. Yilmaz and Ertunc [19] developed a neural network model to predict the tensile strength. The predicted values were found to be in good agreement with the actual values from the experiments. Zhang et al. [4] utilized the external weld appearance technique to describe the morphology of molten pools. Back propagation neural network improved by genetic algorithm (GABP) was established to model the relation between welding appearance and the characteristics of the molten-pool-shadows. The effectiveness of the established model was analyzed at different welding speed. The ANN's prediction performance was verified by experimental results and provided an effective way to predict the weld appearance. Different hybrid methods (e.g. artificial neural network, genetic algorithm, simulated annealing and Quasi Newton line search techniques) were combined to develop three integrated soft computing based ANN-GA, ANN-SA and ANN-Quasi Newton models for modeling and optimization of welding strength for hybrid laser-MIG welded joints of aluminum alloy. Laser power, welding speeds and wires feed rate have been considered as controllable input parameters. These soft computing models employed a trained ANN for calculation of objective function value and thereby eliminated the need of closed form objective function. During optimization based on ANN-GA, it was found that the best performance was observed with absolute percentage error of 0.09% during experimental validation [20]. Luo and Shin [21] estimated the keyhole geometry during laser welding based on a vision system and a radial basis function neural network. To realize the on-line estimation of keyhole dynamics and welding defects, a data-based radial basis function neural network state observer

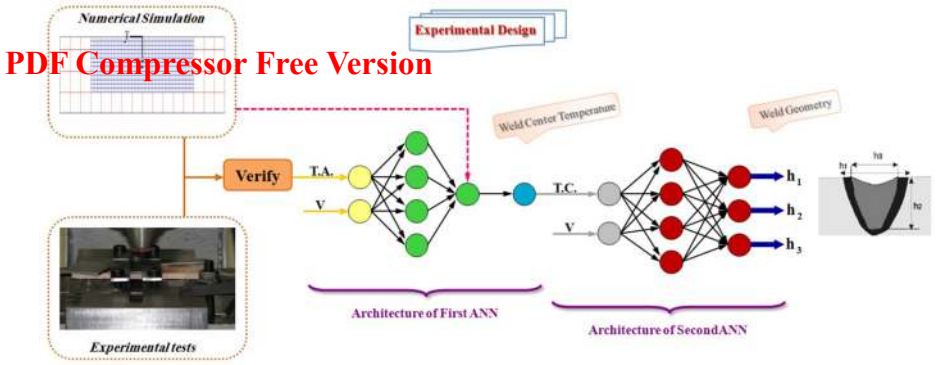

Fig. 1. Weld geometry and temperature distribution procedure using ANN according to experimental and numerical data.

Table 1
Chemical composition of Ti6Al4V as mass percentage.

Al%	V%	Cr%	Cu%	Fe%	Mn%	Mo%	Nb%	Sn%	Zr%	Si%	Ti%
6.5	4.0	<0.01	<0.02	0.04	0.02	<0.03	0.02	<0.05	0.02	0.03	Base

adopted for estimating the penetration depth and the inclination angle in the transient state as welding parameters change suddenly. First, a static neural network was trained in advance to establish a correlation between the welding parameters and unobservable keyhole geometry. The predicted results validated by experimental data which obtained during the welding of stainless steel 304 and magnesium alloy AZ31B. Casalino et al. investigated both CO2 and diode laser welding processes for Ti6Al4V alloy sheet joining using either lap or butt configurations. Artificial neural networks processed the experimental trial data to perform a statistical analysis of the welding parameters effects on the shape of the weld joint [22]. Park and Rhee [23] experimentally investigated laser welding AA5182 aluminum alloy with AA5356 filler wire. The results showed that the tensile strength of the weld was higher than that of the base material under certain conditions. A neural network model was utilized for the prediction of the tensile strength. Genetic algorithm was performed for optimization of the process parameters (laser power, speed and wire feed rate). They reported the proper selection of the process parameters leading to good weldability and productivity. Chang and Na [24] applied the finite element method and artificial neural network for predicting the bead shape in laser spot welding of 304 thin stainless steel. The pulsed Nd:YAG laser spot welding variables (pulse energy, pulse duration, sheet metal thickness, and sheet gaps) were different for various conditions. Sheet thickness, gap size, and bead shape of the workpiece were selected as the input variables for the back-propagation neural network. This combined model of finite element analysis and neural network prepared effective method for the prediction of the bead shapes of the laser spot welds, because the numerical analysis of the laser spot welding for the workpiece with gap between two sheets was limited.

The aim of the present study is to establish a multifunctional predictive method for simultaneous determination of the weld geometry and temperature distribution during the laser welding of Ti6Al4V. The weld geometry characteristics and temperature distribution estimated in a fast and reliable trend under various laser welding conditions by ANN modeling. The temperature results obtained from experimental and numerical approaches were implemented as input parameters and thereby a comprehensive assessment of the weld geometry according to temperature distribution represented as outputs. The ANN results were endorsed by additional untrained experiments.

2. Methodology

According to Fig. 1, laser welding experiments were performed and then numerical simulation was conducted base on the experiments. T.A. and V were considered as input variables for first ANN. The response of the first ANN, T.C. (according to the numerical results), was considered as input variable for the second ANN. Finally, the output of second ANN (weld geometry) was compared with the additional experimental results.

2.1. Laser welding experiments

Experiments were performed to characterize the temperature measurements and HAZ dimensions in laser welding. The sample was Ti6Al4V alloy plate (50 mm × 20 mm with the thickness of 3 mm). The chemical composition of Ti6Al4V alloy (in wt%) is given in Table 1. A pulsed Nd:YAG laser model IQL-20 with maximum mean power of 750 W and wavelength 1.06 μm was used in the welding process. The laser parameter ranges were 0.2–25 ms for pulse duration, 1–1000 Hz for pulse frequency and 0–40 J for pulse energy. The focal point was 6 mm above the surface of the workpiece. The laser spot diameter on the surface of the plate was set at about 0.7 mm during the experiments. The temporal shape of the laser output

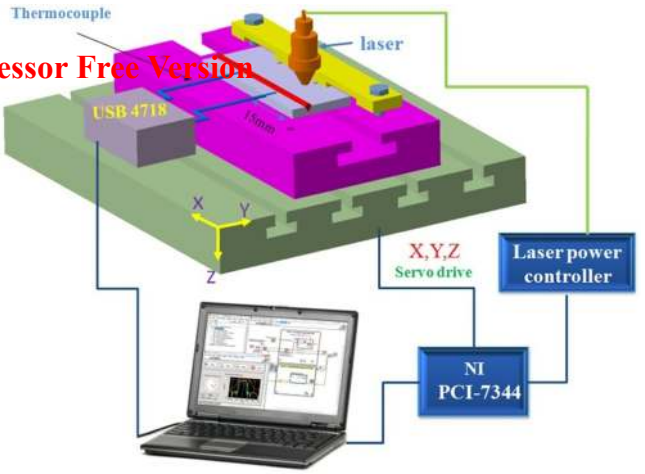

Fig. 2. The schematic diagram of laser welding and monitoring system.

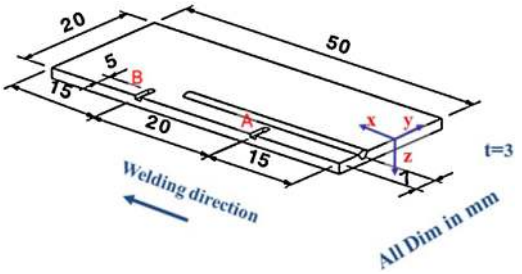

Fig. 3. Schematic model for laser welding.

pulses was like a square. The pure argon gas from a coaxial nozzle was used with the flow rate of 15 l/min for shielding weld zone. Fig. 2 shows a schematic illustration of the experimental setup.

K-type thermocouples with an operative range between −40 °C and +1260 °C and the accuracy of ±1% were used for temperature measurement. Due to the high temperature of the molten pool, the thermocouples were attached on the top surface at 2 mm lateral distance from the center of the molten pool. The locations of the thermocouples are specified in Fig. 3 (points A and B). An automated temperature monitoring system during laser welding was developed by authors group. The system consists of motion controller unit (NI PCI 7344) and data acquisition unit (model: Advantech USB 4718), integrated by using LabVIEW software.

For the metallographic preparation, all the samples were mounted and polished using the standard metallographic techniques (200,400, 600, 800 and 1000 grit) and etched using Kroll0s reagent (Distilled water-92 ml, nitric acid-6 ml and hydro fluoric acid-2 ml). The width and depth of the molten pool were measured using an Olympus SZ-X16 stereoscopic microscope. The Microhardness tester model koopa-MH1 was used for the hardness measurement with load of 200 g and dwell time of 10s.

2.2. Numerical simulation

In this study a thermal numerical simulation was carried out to predict the temperature distribution, geometry of fusion zone (FZ), and HAZ during the laser welding of Ti6Al4V. A schematic configuration of laser welding is shown in Fig. 3.

The origin of an x-y-z coordinate system is chosen at the center of the laser beam on the work piece surface. The laser beam and the coordinate system are fixed and the workpiece moves at the welding speed. The temperature distribution and the melting pool shape not asymmetric. The calculation domain was 50 (mm) × 20 (mm) × 3 (mm) (length × width × thickness). This domain was divided into a non-uniform grid system including a finer mesh and the courser mesh at the weld zone in order to ensure enough numerical precision and the area far from the weld zone in order to reduce the computation cost, respectively. The governing equations (Continuity, momentum and energy) and their boundary conditions were discretized by control volume schemes using the SIMPLE algorithm [25]. In this work, the mathematical formulation of the model is based on the following assumptions:

- The initial temperature for workpiece is at 293 K.

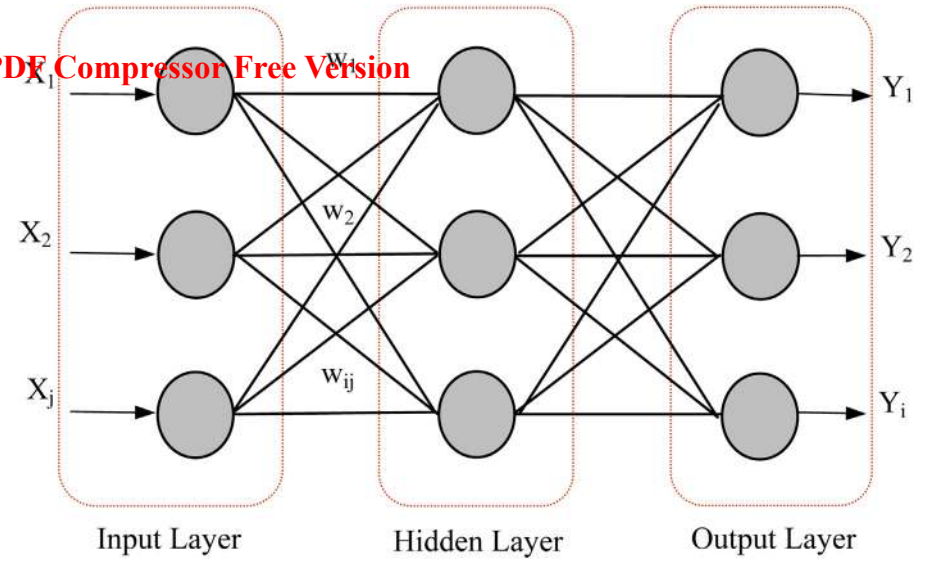

Fig. 4. Architecture of artificial neural network.

- The laser beam and coordinate system are fixed.
- The workpiece moves in the x-direction with a constant velocity, $v_{welding}$.
- All thermophysical properties of the material are temperature dependent.

2.2.1. Boundary and initial conditions

The initial condition at time $t = 0$ is given as

$$T(x, y, z, 0) = 0 \tag{1}$$

The convection and radiation boundary conditions on all surfaces are considered. In addition, on the top surface, a transient heat flux (which is produced by the beam laser) is considered.

$$\text{for z} = 0 \quad -\text{k}\frac{\partial T}{\partial z} = \text{q} - \varepsilon(\text{T})\sigma(T^4 - T_\infty^4) - \text{h}(\text{T} - T_\infty) \tag{2}$$

Where σ is Stefan–Boltzmann constant $= 5.67 \times 10^{8}\,\text{W/m}^2\text{K}^4$, h is the convective heat transfer coefficient, and ε is emissivity. For radiation and convection problems, the following lumped convection coefficient was used as suggested by Frewin and Scott (26):

$$h = 2.4 \times 10^{-3}\varepsilon T^{1.61} \tag{3}$$

2.3. Artificial neural network

An artificial neural network is described by the following features:

I) The architecture that presents the kinds of connections between the layers and neurons.
II) The learning algorithm which determines weights on the connections.
III) The transfer function

Fig. 4 shows the architecture of artificial neural networks. The input of each layer is multiplied by special value called weight. These weights are selected randomly. The output of each layer is calculated by Eq. (4).

$$Y = f(\sum X_j W_{ij} + b) \tag{4}$$

Where W_{ij} is the weight of the connection between each neuron (j) in input layer and each neuron (i) in hidden layer, and also between hidden and output layer. X_j is the value of the input (j) at the input layer, f is the transfer function and b is the bias.

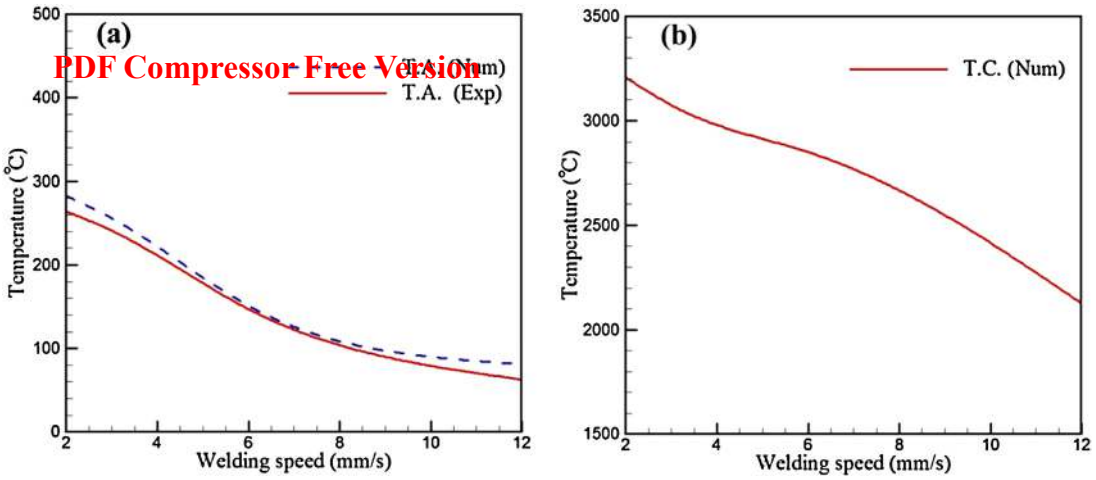

Fig. 5. Maximum temperature versus welding speed, a. around, b. Center.

In this study tan-sigmoid and pureline function were used for hidden and output layers as transfer functions respectively. Eq. (5) depicts the tan-sigmoid transfer function as follow:

$$f(x) = \frac{1}{1 + \exp(-x)} \tag{5}$$

Feed forward back propagation (FFBP) was used as training algorithm in both artificial neural networks. All computations were carried out with MATLAB (version 7.10.0.499) mathematical software. Temperature around (TA) and welding speed (V), for the first ANN model, and temperature center (T.C.) and weld speed (V), for second ANN were used as input variables and temperature center and geometric parameters (h_1, h_2 and h_3) were used as outputs variables for first and second ANNs respectively. 32 Experimental points were employed to feed the model. The data set was derived to training and test sets which contained 80 and 20 percent of data points respectively. According to Eq. (6), all data points were to be scaled into the range of (-0.9, 0.9) due to using tan-sigmoid transfer function.

$$X_{norm} = 1.8\frac{X - X_{\min}}{X_{\max} - X_{\min}} - 0.9 \tag{6}$$

3. Results and discussion

3.1. Verification

The numerical results for the temperature around of the molten pool obtained from the finite volume model were compared with the experimental data and good agreement was observed as shown in Fig. 5a. Furthermore, the weld center temperature in molten pool region, obtained from the numerical model, is represented in Fig. 5b.

Due to the difficulties that associated with the experimental measurements of the center point cooling rate in the molten pool region, the numerical model was used for estimation of the weld fusion zone cooling rates at several welding speeds as shown in Fig. 6.

During laser welding of the Ti6Al4V alloy, the phase transformation of the fusion zone is proportional to the cooling rate during laser welding [6]. The phases transformations occurrence in the fusion zone are the α-to-β phase transformations during the heating stage and the β-to-α phase transformation during the cooling stage. The FZ microstructure consists of an acicular martensitic α' solidification structure within the prior-β grains as observed in Fig. 7a. According to Fig. 7b, it is observed that in the regions of HAZ near FZ, the high peak temperature and faster cooling rate result in the disappearance of the original α phase and the appearance of large amount of martensite α' that can be considered to be the transformed region. As observed in Fig. 7b, some retained original α phase can be found. This trend is also demonstrated by Gao et al. [5]. For the part of the HAZ near base metal, the partially α-to-β transformation is occurred due to low peak temperature (see Fig. 7c).

According to the obtained results in Fig. 6, the cooling rate of the weld center point at the welding speed of 9 mm/s, is estimated to be 100 °C/s and sufficient for martensitic transformation in Ti6Al4V. As shown in Fig. 8, the critical cooling rate for α′ martensite formation is identified to be 410 °C/s. The cooling rates between 20 and 410 °C/s produce a block, diffusionlessly transformed, massive martensitic structure αm (see Fig. 8). The αm is chemically and crystallographically identical to α′ with lower hardness vs. acicular α′ [6].

Changing the welding speed from 3 to 9 mm/s produced slightly different cooling rates for the temperature ranges from the melting point to 1100 °C. The cooling rate for the temperature range of 1100–600 °C is about 80 °C/s for welds between

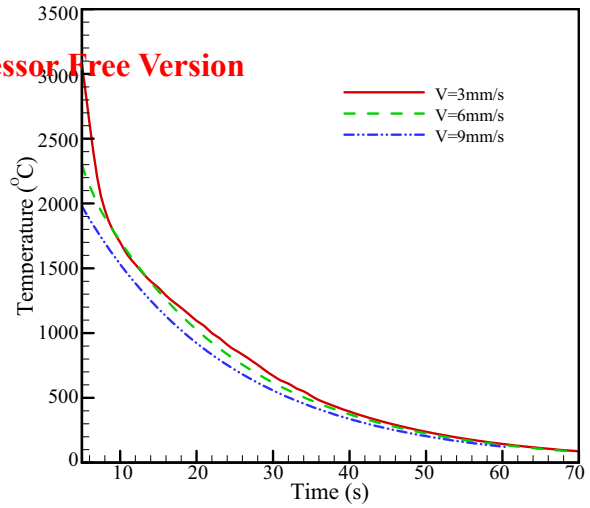

Fig. 6. Finite volume model predicted center point cooling rates of the molten pool at different laser welding speeds.

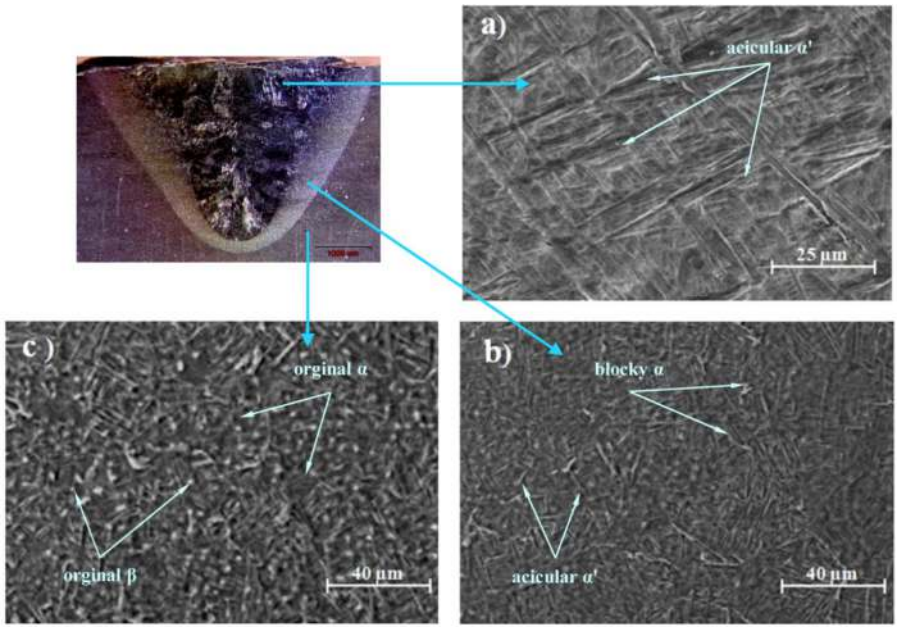

Fig. 7. Metallographic images from weld cross section at welding speed of 6 mm/s.

3 and 9 mm/s welding speeds. At speed from 3 to 9 mm/s the weld fusion zones transforms to martensite, while leaving a small percentage of retained β as observed in this research.

According to the results in Fig. 9, for the welded samples with the welding speed of 3 mm/s, the cooling rate is estimated to be 50 °C/s. This cooling rate is slower than the samples with welding speed of 9 mm/s. However, it is still fast enough to enable partial formation of αm martensite.

Fig. 9 shows the micro-hardness distribution of the weld joint cross section under different welding speeds. At two different welding speeds the average hardness of FZ is shown in the weld center. As observed in Fig. 9, the mean values of the micro-hardness in the FZ decrease slightly with increasing the welding speed. This trend is related to the increase of the cooling rate at high welding speed [6].

The cross sections micro-hardness of the as-welded samples reveal that the micro-hardness has the lowest values of 330 ± 10 HV in the BM region and the highest values are obtained in the FZ that concentrated about 385 HV in the center of the weld joint. The hardness in the HAZ decreased sharply with increasing distance from FZ.

For high welding speed, the hardness values in the HAZ decreases sharply when the moving from position of the FZ/HAZ interface to the HAZ/BM interface.

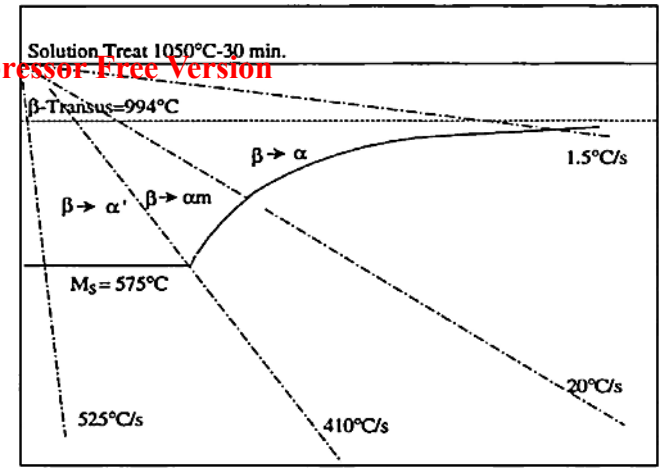

Fig. 8. Schematic continuous cooling temperature transformation diagram for TI6Al4V beta solution treated at 1050 °C for 30 min [6].

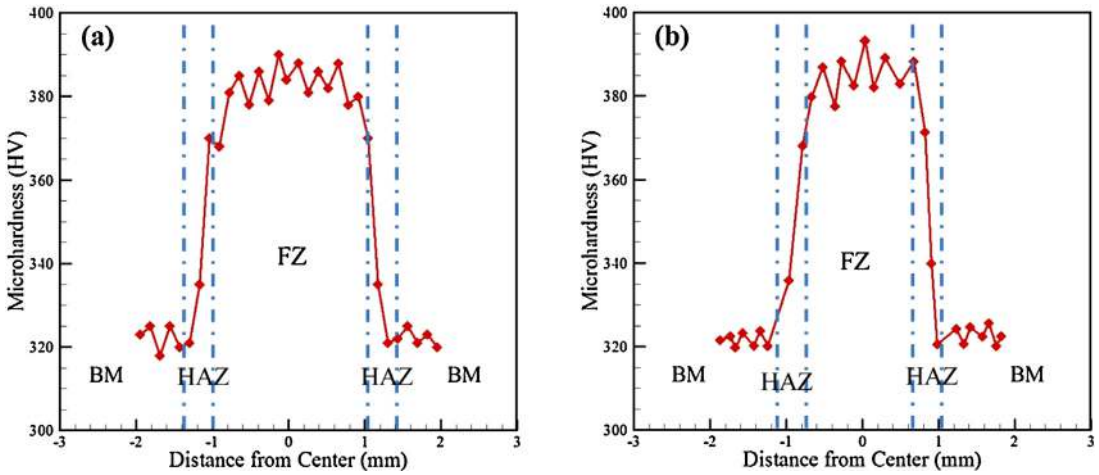

Fig. 9. Micro-hardness distribution of the weld cross section at two welding speeds: (a) v = 3 mm/s, (b) v = 6 mm/s.

Table 2
Ranges of process variables.

Variables	Ranges
Laser Travel Speed (mm/s)	2–12
Temperature Around (°C)	63–264
Temperature Center (°C)	2125.6–3160.3
h_1 (mm)	1.74–2.74
h_2 (mm)	0.87–1.82
h_3 (mm)	1.468–2.2

3.2. Artificial neural network

The input variables of the first trained ANN are V and T.A. and the output variable is T.C. For the second trained ANN, the input variables are V and T.C. and the outputs are geometric parameters (h1, h2 and h3). Table 2 indicates the ranges of these parameters.

Topology of both ANNs is illustrated in Fig. 10. It can be seen that the number of layers, neurons of each layer, and the interconnection of the neurons between the layers. The aim of ANNs training is to obtain the best weights with the minimum values of prediction error.

Optimized ANNs by considering minimum prediction error were obtained by changing the number of neurons in the hidden layer, transfer functions and repetition of training step. In order to find the best number of neurons in hidden layers, various topologies have been studied. Fig. 11 shows the error of each topology by changing of the number of neurons in

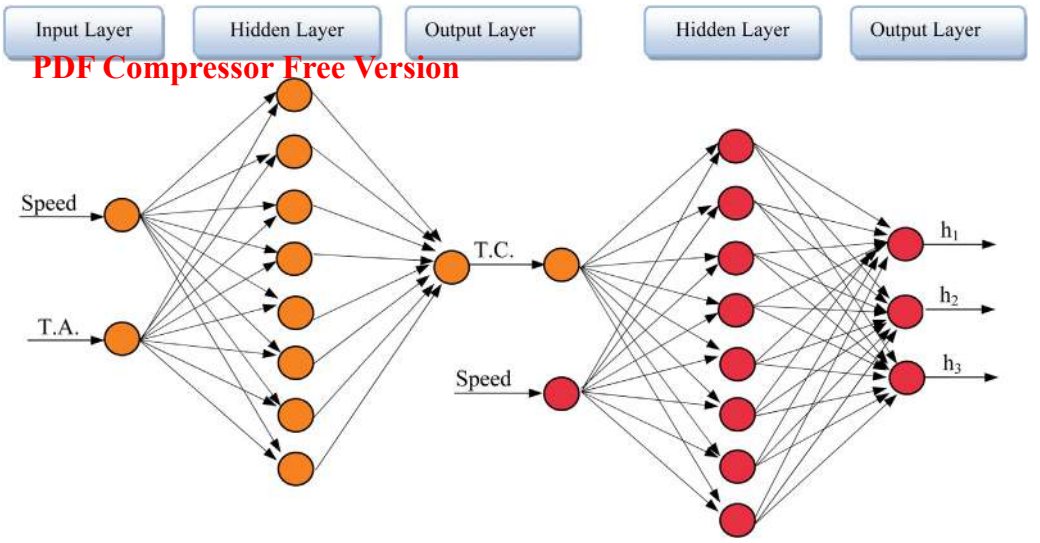

Fig. 10. Optimized topology of artificial neural network.

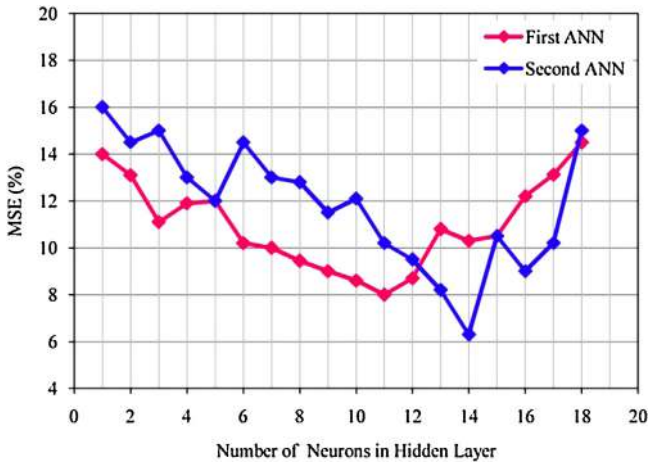

Fig. 11. The mean square error based on variation of neurons in hidden layer.

Table 3
Comparison between the experimental and ANN results of temperature distribution for test data set.

Factors			Temperature center (°C)		
No.	Welding speed (mm/s)	Temperature around (°C)	Experimental	ANN Model	APE (%)
1	3	240.2	3072.4	3070.0	0.991
2	5.2	169.1	2913.7	2915.6	1.153
3	7.6	115.7	2693.3	2694.4	0.994
4	9.6	95.4	2463.5	2462.6	0.891
5	11.2	80.0	2243.0	2242.1	1.076
				MAPE (%)	1.021

hidden layer. It can be seen that artificial neural networks with 11 and 14 neurons in hidden layers have minimum values of mean square error (MSE). The Eq. (7) represented the MSE function as follow:

$$MSE = \frac{1}{N}\sum_{i=1}^{N}\left(Y_{pre} - Y_{ex}\right)^2 \tag{7}$$

Where Y_{ex} is the experimental output, Y_{pre} is the network output and N is the number of data points.

Table 4
Comparison between the experimental and ANN results of weld geometry for test data set.

Factors			h_1 (mm)			h_2 (mm)			h_3 (mm)		
No.	Welding speed (mm/s)	Temperature center (°C)	Exp.	ANN	APE (%)	Exp.	ANN	APE (%)	Exp.	ANN	APE (%)
1	3	3072.4	2.56	2.58	0.960	1.71	1.73	0.968	2.10	2.12	0.942
2	4.6	2958.4	2.31	2.33	0.843	1.53	1.55	0.957	1.90	1.92	0.931
3	7.2	2738.1	2.02	2.04	1.039	1.23	1.25	0.986	1.68	1.70	0.938
4	9.2	2526.5	1.90	1.92	0.935	1.03	1.05	0.983	1.62	1.64	0.929
5	11	2266.5	1.80	1.82	0.888	0.92	0.92	0.828	1.52	1.54	1.007
			MAPE(%)		0.933			0.944			0.949

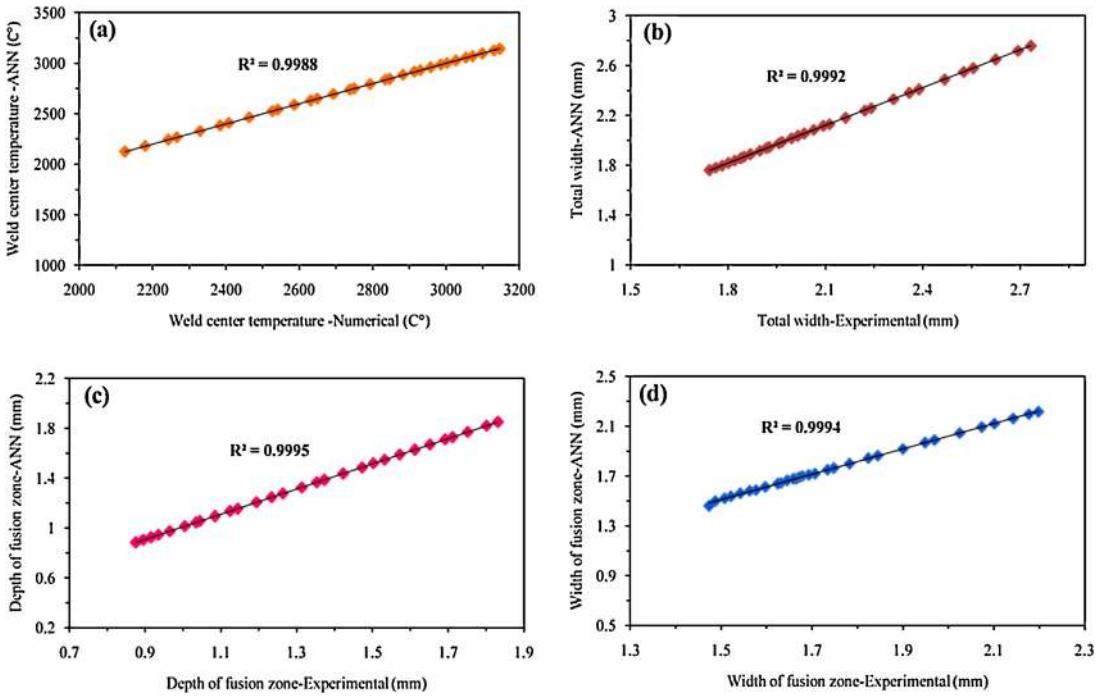

Fig. 12. ANN regression diagrams of output parameters: (a) weld center temperature, (b) total width, (c) depth of fusion zone and (d) width of fusion zone.

The accuracy of ANNs was examined using test data sets (Tables 3 and 4). Test data sets were selected from the experimental points randomly that was not used during training step. The mean absolute percentage error (MAPE) of T.C, h1, h2 and h3 are 1.021, 0.933, 0.944 and 0.949 respectively. These values indicate high accuracy of the models.

Fig. 12 compares the predicted values of ANN models with experimental and numerical data sets for weld center temperature, h1, h2, and h3 parameters at different speeds and temperature distribution. It can be observed that the predicted values obtained from the ANN models are in good agreement with the experimental and numerical data for all cases. Moreover, the R2 value of 0.999 for all cases confirms good performance of the trained networks.

Also, the outline of the process parameters was investigated during laser welding of Ti6Al4V. Fig. 13 depicts the effect of welding speed and the resultant temperature on weld geometry assessment factors. By increasing the welding speed, the width and depth of fusion zone decreased. Also, by reduction of temperature in the fusion zone, the width and depth of fusion zone decreased. It can be concluded that the temperature distribution in the fusion zone is an appropriate factor for evaluation of the weld geometry. Moreover, the predicted results of ANNs are in good agreement with experimental results which demonstrates the minimum mean square error of ANN models for the laser welding process.

4. Discussion

The weld geometry has been quantitatively investigated through experimental and numerical analysis of laser welding of Ti6Al4V alloy. The numerical simulation results for the temperature distribution in the weld pool and HAZ regions were in good agreement with the experiments data. The Numerical results for temperature distribution used as a suitable criterion for estimating the size of the weld cross section (depth and width) during laser welding. Furthermore, the numerical model was used for prediction of cooling rate at the center of the weld and characterization of fusion zone microstructure. There are some difficulties in measuring and predicting the size of the weld pool region. In this paper, the temperature distribution

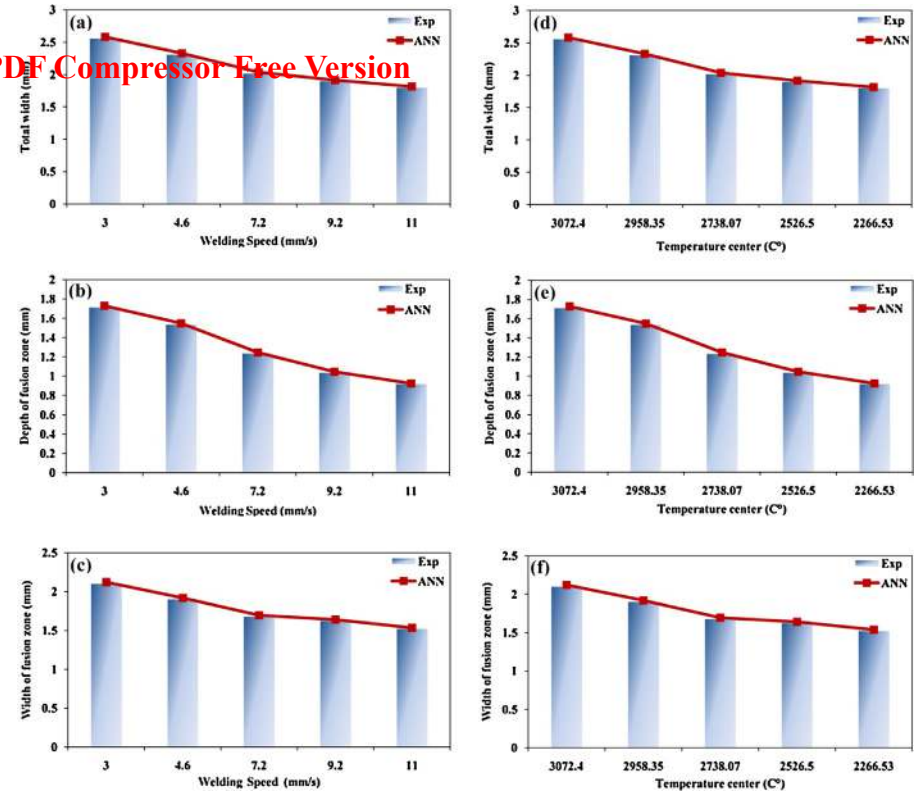

Fig. 13. Effect of welding speed on weld geometry: (a) total width, (b) depth of fusion, (c) width of fusion zone, effect of temperature on weld geometry (d) total width, (e) depth of fusion, (f) width of fusion zone.

was used as an indirect approach for prediction of the geometry and the size of the weld pool and HAZ regions. The results showed that by changing the welding speed, the rate of the input energy at the constant time incident to the workpiece varied and consequently the temperature of the fusion zone and its surroundings will change. As the temperature changes, the heating and cooling cycles will change and affect the weld pool growth, the resultant microstructure and mechanical properties. By variation of the laser welding speed in the range of 2 mm/s–12 mm/s, by increasing the welding speed, the maximum temperature in the fusion zone, HAZ and its adjacent regions are decreased. Owing to the difficulties in temperature measurement of the molten pool in the experiments, the adjacent molten pool regions temperature was measured and the temperature distribution of the molten pool was predicted using the numerical simulations. Meanwhile, the phase transformation in the fusion zone and HAZ regions was evaluated according to the predicted cooling curve from numerical simulations and the continuous cooling transformation diagram for Ti6Al4V alloy. Thereby, the results were compared with the experimental investigation through microstructure of the weld. The results showed that the numerical model can estimate the cooling rate in an appropriate manner and explain the microstructure changes of the Ti6Al4V alloy that influenced by heating and cooling cycles. In order to save the time and costs for accurate prediction of the weld geometry, the process was simulated based on artificial neural network. To this aim, two different ANNs were trained for progressive prediction of the temperature distribution in weld pool region and the weld geometry. The first ANN was trained by V and T.A. parameters as inputs to predict the T.C. which was obtained by numerical results. In the second ANN, V and T.C. were considered as input parameters and weld geometry (h1, h2, and h3) were predicted. Both of ANNs were trained by feed forward back propagation algorithm. Tansig and pureline transfer functions were utilized in hidden and output layers respectively. The number of neurons in hidden layer was obtained by trial and the error which had the mean square error of 0.079 and 0.063 for the first and the second ANNs respectively. The correlation coefficient (R2) of output parameters, by values of 0.9988, 0.9992, 0.9995, and 0.9994 were obtained for T.C., h1, h2, and h3 respectively which represented the high accuracy of the predicted results. Moreover, the mean absolute percentage error of the ANN results and experimental tests was indicated the good performance of trained networks. Finally, it was observed that neural networks can be used as a powerful tool to predict the temperature distribution and weld geometry in laser welding process and has the potential to eliminate the need of further experimental tests.

5. Conclusions

The weld cross section geometry in laser welding of Ti6Al4V alloy has been determined through methods of experiment, numerical simulation and artificial neural network. The temperature distribution was exerted as an indirect approach for estimating the size of the melt pool profile and HAZ region. The conclusions from the foregoing analyses are as follows:

- By changing the welding speed, the rate of input energy to the fusion zone and its surroundings will change. Therefore, the heating and cooling cycles will change and affect the melt pool growth and the resultant microstructure. During laser welding of Ti6Al4V, the cooling rate of weld center point is sufficient for martensitic transformation in weld fusion zones.
- Different ANNs were developed for progressive prediction of the melt pool temperature distribution and the weld geometry at lower time and cost in comparison with experimental and numerical simulation.
- The applied ANN models could successfully predict the process with average mean absolute percentage error (MAPEs) of 0.962 and determination coefficients (R2) of 0.999 for all cases. The performance of the proposed method in temperature distribution and weld geometry was satisfactory. The results indicated that ANN outputs are in good agreement with the experimental and numerical data which implies the high potential of ANN in prediction of the proposed process.

References

[1] G. Casalino, M. Mortello, N. Contuzzi, F.M.C. Minutolo, Finite element model for laser welding of titanium, Procedia CIRP 33 (2015) 435–440.
[2] F. Kong, R. Kovacevic, 3D finite element modeling of the thermally induced residual stress in the hybrid laser/arc welding of lap joint, J. Mater. Process. Technol. 210 (2010) 941–950.
[3] M. Moradi, M. Ghoreishi, J. Frostevarg, A.F.H. Kaplan, An investigation on stability of laser hybrid arc welding, Opt. Lasers Eng. 51 (2013) 481–487.
[4] Y. Zhang, X. Gao, S. Katayama, Weld appearance prediction with BP neural network improved by genetic algorithm during disk laser welding, J. Manuf. Syst. 34 (2015) 53–59.
[5] X.-L. Gao, L.-J. Zhang, J. Liu, J.-X. Zhang, Effects of weld cross-section profiles and microstructure on properties of pulsed Nd:YAG laser welding of Ti6Al4V sheet, Int. J. Adv. Manuf. Technol. 72 (2014) 895–903.
[6] P.-q. Xu, L. Li, C. Zhang, Microstructure characterization of laser welded Ti-6Al-4V fusion zones, Mater. Charact. 87 (2014) 179–185.
[7] G. Mi, Y. Wei, X. Zhan, C. Gu, F. Yu, A coupled thermal and metallurgical model for welding simulation of Ti-6Al-4V alloy, J. Mater. Process. Technol. 214 (2014) 2434–2443.
[8] M.J. Torkamany, F. Malek Ghaini, R. Poursalehi, Dissimilar pulsed Nd:YAG laser welding of pure niobium to Ti-6Al-4V, Mater. Des. 53 (2014) 915–920.
[9] R. Wang, Y. Lei, Y. Shi, Numerical simulation of transient temperature field during laser keyhole welding of 304 stainless steel sheet, Opt. Laser Technol. 43 (2011) 870–873.
[10] C. Wei, J. Zhang, S. Yang, W. Tao, F. Wu, W. Xia, Experiment-based regional characterization of HAZ mechanical properties for laser welding, Int. J. Adv. Manuf. Technol. 78 (2015) 1629–1640.
[11] S. Shakeri, A. Ghassemi, M. Hassani, A. Hajian, Investigation of material removal rate and surface roughness in wire electrical discharge machining process for cementation alloy steel using artificial neural network, Int. J. Adv. Manuf. Technol. (2015) 1–9.
[12] M. Shirani, A. Akbari, M. Hassani, Adsorption of cadmium(ii) and copper(ii) from soil and water samples onto a magnetic organozeolite modified with 2-(3,4-dihydroxyphenyl)-1,3-dithiane using an artificial neural network and analysed by flame atomic absorption spectrometry, Anal. Methods 7 (2015) 6012–6020.
[13] S.M. Karazi, A. Issa, D. Brabazon, Comparison of ANN and DoE for the prediction of laser-machined micro-channel dimensions, Opt. Lasers Eng. 47 (2009) 956–964.
[14] J. Lee, K. Um, A comparison in a back-bead prediction of gas metal arc welding using multiple regression analysis and artificial neural network, Opt. Lasers Eng. 34 (2000) 149–158.
[15] K. Maji, D.K. Pratihar, A.K. Nath, Laser forming of a dome shaped surface: experimental investigations, statistical analysis and neural network modeling, Opt. Lasers Eng. 53 (2014) 31–42.
[16] Y. Rong, Z. Zhang, G. Zhang, C. Yue, Y. Gu, Y. Huang, C. Wang, X. Shao, Parameters optimization of laser brazing in crimping butt using Taguchi and BPNN-GA, Opt. Lasers Eng. 67 (2015) 94–104.
[17] X. Wang, C. Zhang, P. Li, K. Wang, Y. Hu, P. Zhang, H. Liu, Modeling and optimization of joint quality for laser transmission joint of thermoplastic using an artificial neural network and a genetic algorithm, Opt. Lasers Eng. 50 (2012) 1522–1532.
[18] P. Sathiya, K. Panneerselvam, M.Y. Abdul Jaleel, Optimization of laser welding process parameters for super austenitic stainless steel using artificial neural networks and genetic algorithm, Mater. Des. 36 (2012) 490–498.
[19] M. Yilmaz, H.M. Ertunc, The prediction of mechanical behavior for steel wires and cord materials using neural networks, Mater. Des. 28 (2007) 599–608.
[20] S. Chaki, B. Shanmugarajan, S. Ghosal, G. Padmanabham, Application of integrated soft computing techniques for optimisation of hybrid CO2 laser-MIG welding process, Appl. Soft Comput. 30 (2015) 365–374.
[21] M. Luo, Y. Shin, Estimation of keyhole geometry and prediction of welding defects during laser welding based on a vision system and a radial basis function neural network, Int. J. Adv. Manuf. Technol. (2015) 1–14.
[22] G. Casalino, F. Curcio, F. Memola Capece Minutolo, Investigation on Ti6Al4V laser welding using statistical and Taguchi approaches, J. Mater. Process. Technol. 167 (2005) 422–428.
[23] Y. Park, S. Rhee, Process modeling and parameter optimization using neural network and genetic algorithms for aluminum laser welding automation, Int. J. Adv. Manuf. Technol. 37 (2008) 1014–1021.
[24] W.S. Chang, S.J. Na, Prediction of laser-spot-weld shape by numerical analysis and neural network, Metall. Mater. Trans. B 32 (2001) 723–731.
[25] M. Akbari, S. Saedodin, D. Toghraie, R. Shoja-Razavi, F. Kowsari, Experimental and numerical investigation of temperature distribution and melt pool geometry during pulsed laser welding of Ti6Al4V alloy, Opt. Laser Technol. 59 (2014) 52–59.